Journal of Materials Chemistry

Cite this: *J. Mater. Chem.*, 2011, **21**, 2344

www.rsc.org/materials

PAPER

Highly reproducible synthesis of hollow gold nanospheres with near infrared surface plasmon absorption using PVP as stabilizing agent

Sandra Preciado-Flores,†[a] Danchen Wang,†[ab] Damon A. Wheeler,[a] Rebecca Newhouse,[a] Jennifer K. Hensel,[a] Adam Schwartzberg,[c] Lihua Wang,[d] Junjie Zhu,[b] Marcelino Barboza-Flores[e] and Jin Z. Zhang*[a]

Received 29th October 2010, Accepted 23rd November 2010
DOI: 10.1039/c0jm03690k

An improved synthetic method has been designed and demonstrated to reproducibly generate hollow gold nanospheres (HGNs) with strong surface plasmon resonance (SPR) absorption in the near infrared (NIR). The HGNs have been synthesized *via* galvanic replacement of cobalt with gold while utilizing different amounts of poly(vinylpyrrolidone) (PVP) as a template stabilizing agent. Ninety percent of syntheses performed by this modified method resulted in HGNs with an SPR near 800 nm, which is highly desirable for biomedical applications such as photothermal ablation (PTA) therapy, while other polymers (PAA and PEG) did not. Based on absorption and TEM measurements, PVP stabilizes the cobalt template particles *via* carbonyl-induced stabilization that slows nucleation and growth of the gold shell allowing for the generation of a reproducibly thin shell, thereby inducing a significant red shift of the SPR to 800 nm. The results are significant to various potential applications of HGNs, *e.g.* cancer therapy and sensing.

Introduction

Gold and silver nanoparticles exhibit unique optical and electronic properties as a result of the collective oscillation of their conduction band electrons. When the frequency of the incident light matches the intrinsic electron oscillation frequency, the particles absorb the light efficiently, resulting in the observed surface plasmon resonance (SPR).[1–3] The SPR depends on a combination of factors including size, imbedding medium, and most importantly, shape.[4] The combination of different surfactants and seed-mediated growth methods used in colloidal synthesis has given a high degree of control and produced diverse metal nanostructures with various shapes, including rods,[5,6] prisms,[7] cubes,[7] triangles,[8] cages,[9] aggregates,[10] and frames,[11] as well as many others.

A particularly interesting metal nanostructure is the hollow gold nanosphere (HGN), consisting of a spherical gold shell filled with the imbedding medium.[12] In HGNs, the ratio of the shell diameter and thickness (defined as the aspect ratio of the nanostructure) determines the peak position of the SPR and their uniformity determines the bandwidth of the SPR.[4,13] Similarly gold nanoshells fabricated by growing gold nanoparticles on a silica core have been previously synthesized and characterized.[14,15] Silica in these cases acts as a template which remains in the final nanostructure unless removed by chemical agents. Likewise, sacrificial templates such as silver and cobalt nanoparticles can be employed to synthesize hollow gold nanostructures with an empty interior since silver or cobalt can spontaneously reduce gold ions in a ratio which ensures more template atoms are oxidized than gold atoms reduced. Sun *et al.* have successfully used various silver nanostructures to create hollow gold nanomaterials.[16,17] Cobalt was first demonstrated successfully as a sacrificial template to create HGNs by Liang *et al.*[18] The synthesis was later improved by Schwartzberg *et al.* to create nearly homogeneous and monodisperse HGNs with SPR readily tunable over the entire visible to NIR regions.[13]

The highly tunable SPR makes HGNs ideal for applications in molecular sensing based on surface enhanced Raman scattering (SERS),[13,19,20] DNA biosensor fabrication,[21] biomedical imaging, and cancer treatments based on photothermal ablation (PTA).[22–24] For PTA in particular, nanostructures with NIR SPR are strongly desired due to deep tissue penetration in the NIR.[24] Similar nanostructures, such as core/shells, nanorods, metallic nanocomposites and bimetallic systems, have been studied for fluorescence enhancement,[25] catalysis,[26] gene delivery,[26] and other biomedical applications.[27–29] Similar to other gold nanostructures, HGNs can be readily functionalized with virtually any thiol-terminated moiety by employing well-studied gold–thiol surface chemistry techniques. Gold is also

[a]*Department of Chemistry and Biochemistry, University of California, Santa Cruz, CA, 95060, USA. E-mail: zhang@chemistry.ucsc.edu; Tel: +1 831 459 3776*
[b]*School of Chemistry and Chemical Engineering, Nanjing University, Nanjing, 210093, PR China*
[c]*The Molecular Foundry, Lawrence Berkeley National Labs, Berkeley, CA, 94720, USA*
[d]*Department of Chemistry and Biochemistry, Kettering University Flint, MI, 48504, USA*
[e]*Centro de Investigación en Física de la Universidad de Sonora, Apartado Postal 5-088, Hermosillo, Sonora, 83190, Mexico*
† These authors made equal contribution to this work.

preferred for biological applications, since its inert nature and resistance to oxidation allow for biocompatibility, in contrast to silver.

A special interest concerning HGNs is in their potential use for PTA therapy of cancer, since they possess a relatively low thermal mass due to their thin shells which allow them to dissipate the heat to their local environment efficiently. This has been successfully demonstrated both *in vitro* and *in vivo* studies of human squamous carcinoma[22] and melanoma in live mice.[23] For biological applications, in particular, the size and shape of the nanostructures are very important considerations. For instance, nanostructures larger than 100 nm do not easily penetrate the cell membrane and at the lower limit, structures with dimensions less than 20 nm readily diffuse out of cells.[30] While gold/silica nanoshells are typically greater than 100 nm in diameter,[31] the HGNs with NIR absorption can be synthesized with outer diameter between 25 and 50 nm, and are therefore ideal for biological applications, *e.g.* as an efficient photothermal coupling agent for PTA.[24] Even though the HGNs are attractive due to their unique combination of small size, spherical shape, and strong, narrow and tunable NIR SPR, their synthesis is challenging in terms of reproducibility, especially those with SPRs in the desired NIR (*e.g.* 800 nm) region. This is because HGNs with 800 nm SPR require relatively large diameter and thin shell that turn out to be more difficult to create with the Co-template-based synthesis.[13]

The above challenge has led us to search for a more reproducible method for synthesizing HGNs with NIR SPR. We hypothesized that stabilizing the Co template and slowing down the nucleation and growth of the gold shell could perhaps lead to the creation of larger and thinner gold shells that correspond to NIR SPR. The introduction of a polymer in the synthesis, such as poly(vinylpyrrolidone) (PVP), has been studied as an efficient stabilizing agent for colloidal nanoparticles,[32–34] metallic shape confining,[35,36] and for the synthesis of long, aligned structures of HGNs.[26,37] However, a systematic and reproducible synthesis of HGNs with strong absorption in the NIR (750–810 nm) has not been reported previously.

Herein, we report a greatly improved synthesis of HGNs in terms of reproducibility by the inclusion of PVP as a stabilizing agent. These resultant HGNs with an SPR at NIR wavelengths also show high stability at ambient conditions, and appropriate size for biomedical applications. A complete study and analysis of the results have been carried out to gain insight into the role of PVP in the reproducible synthesis of HGNs.

Methods and materials

Synthesis

Hollow gold nanospheres (HGNs) were synthesized following previously reported protocols,[13] with some modifications. The synthesis was carried out using air free methods to reduce premature oxidation of the cobalt particles. Additionally, all glassware that was used was cleaned thoroughly with Alconox®, aqua regia, and ultrapure water.

In a 500 mL two-necked round-bottom flask, 100 mL of ultrapure (18 MΩ) water was combined with 100 μL of 0.4 M cobalt chloride hexahydrate ($CoCl_2 \cdot 6H_2O$) and 400 μL of 0.1 M sodium citrate trihydrate ($Na_3C_6H_5O_7 \cdot 3H_2O$). The solution was deaerated by bubbling with argon gas for 40 minutes with no magnetic stirring. To that solution, 100 μL of 1.0 M sodium borohydride ($NaBH_4$) was injected, and the solution turned from a pale pink color to brown over the course of a few seconds indicating the formation of cobalt nanoparticles. Simultaneously, 100–900 μL of a 1 wt% solution of poly (vinylpyrrolidone) $(C_6H_9NO)_n$ (Scheme 1a), with an average M_w of 55 000, was injected; which is similar to that used in previous studies for shape-controlled synthesis of gold and silver nanoparticles.[38,39]

The as-formed cobalt nanoparticle solution was further deaerated by passing argon through the reaction flask for a further 40 minutes until the evolution of H_2 bubbles ceased, indicating the complete hydrolysis of borohydride.

Subsequently, 30 mL of the cobalt nanoparticles were transferred to a 100 mL beaker and immediately added to a stirring solution of 10 mL of ultrapure water and 15 μL of 0.1 M chloroauric acid trihydrate ($HAuCl_4 \cdot 3H_2O$) (Scheme 1b and c), allowing the formation of $CoCl_2$ and the reduction of Au^{3+} (Scheme 1d). The solution was allowed to stir for another five minutes under ambient conditions to allow the complete oxidation of any unreacted cobalt (Scheme 1e) and a slow change in color from brown to green indicates that the formation of hollow gold spheres was completed (Scheme 1f).

The synthesis was also performed with poly(acrylic acid) (PAA, M_w = 100 000) and polyethylene glycol (PEG, M_w = 10 000), respectively, and the concentration of $NaBH_4$ was decreased to 0.1 M, while other reagents and steps in the synthesis were kept identical. A total of 29 syntheses were performed with PVP, and 20 without PVP for comparison. The average diameter and shell thickness of HGNs for each sample are estimated from HRTEM images.

Measurement and characterization

UV-Vis absorption measurements were carried out using a Varian Cary 50 UV-Visible spectrometer with a spectral resolution of 2 nm. Samples were concentrated using a Sorvall RC 5C Plus super-centrifuge which was spun at 14 000 rpm for 15 minutes at

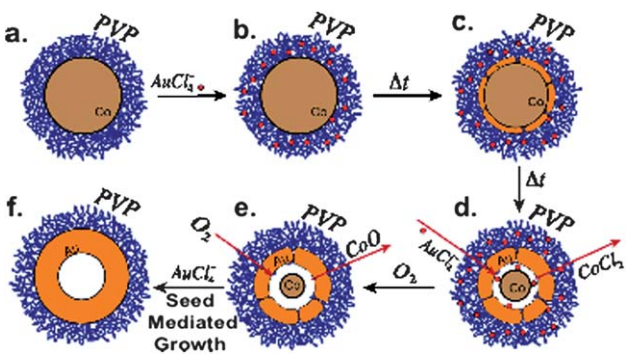

Scheme 1 Schematic illustration of the HGN synthesis with PVP as stabilizing agent. (a) Attachment of PVP on Co nanoparticles surface; (b) interaction of $AuCl_4^-$ with Co nanoparticles; (c) reduction of Au^{3+} by Co^0; (d) initialization of the gold shell formation; (e) oxidation of remaining Co nanoparticles; and (f) formation of hollow gold nanospheres with the presence of PVP.

a constant temperature of 20 °C. Low-resolution transmission electron microscopy (TEM) was carried out using a JEOL model JEM-1200EX microscope. High-resolution transmission electron microscopy (HRTEM) was performed on a Philips CM300-FEG at the National Center for Electron Microscopy at Lawrence Berkeley National Laboratory and the particle size was analyzed using image-J software.[40]

Results and discussion

The primary goal of this work is to develop a simple and highly reproducible method for synthesizing HGNs with strong SPR in the NIR for biological and other applications. Attempts to reproduce the HGNs reported previously from our lab, which showed desirable optical properties for PTA therapy,[41] had resulted largely in HGNs with SPR in the visible region and a small percentage with SPR in the NIR. In the process of this work we determined that the addition of a more robust stabilizing agent could: (a) stabilize larger cobalt particles formed with low concentrations of sodium citrate (which, without PVP, often results in flocculation) and (b) kinetically control the formation of the gold shell, a normally fast process, making thinner (and thus more red-shifted) shells possible. Key steps of the synthesis are illustrated schematically in Scheme 1.

With the addition of PVP, a common metal colloid stabilizing polymer, we first observed a significant and highly reproducible SPR in the NIR region of the resulting HGNs, as shown in a representative absorption spectrum in Fig. 1a. It is important to recall that the SPR position of the HGNs can be tuned to cover the entire visible to NIR by changing the diameter and wall thickness.[41–43]

The spectrum is consistent with previously reported HGN solutions, if somewhat broadened. This may be due to several effects. First, the reaction parameters have not been fully optimized for high homogeneity but instead for NIR absorption. Second, the HGN shell thickness shown here is less than those previously reported. As a result, the homogeneous linewidth may be significantly broadened. Third, there are larger variations in shell diameter and thickness that cause inhomogeneous broadening to the observed SPR. However, the slightly broad SPR is a not a key issue in this study and it is possible to reduce it though systematic optimization if desired.

To determine reproducibility and demonstrate the significant red-shift observed in the SPR, the synthesis was repeated multiple times both with (29 syntheses) and without (20 syntheses) PVP added to the reaction. These results are compiled in Fig. 1b, which shows the SPR maximum absorption position and FWHM (inset) of both the PVP (red) and non-PVP synthesized HGNs (blue). The average SPR absorption maximum of the HGNs synthesized with PVP is 1.64 ± 0.14 eV (760 ± 59.7 nm), with an average FWHM of 0.53 ± 0.15 eV (237 ± 58 nm) and the non-PVP HGNs yielded an average SPR position of 2.1 ± 0.1 eV (602 ± 29.0 nm) and FWHM of 0.38 ± 0.07 eV (112 ± 26 nm). As the histogram indicates, the shift in SPR absorption is significant, approximately 0.46 eV (158 nm), and is achieved by changing nothing more than the addition of supplemental stabilizing moieties to the cobalt particles. Fig. 2a and b correlate the FWHM and SPR positions observed in PVP and non-PVP derived HGNs, respectively. The HGNs

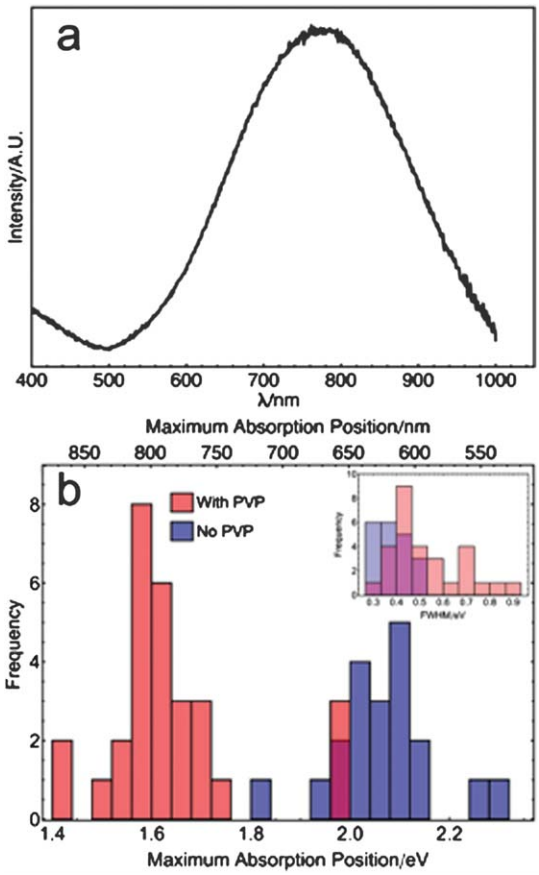

Fig. 1 (a) UV-Vis absorption of a representative HGN sample synthesized with PVP as stabilizing agent. (b) Histograms that indicate the maximum absorption position and FWHM (inset figure) of 29 HGNs synthesized with PVP (pink bars) and no PVP (blue bars). The two bar colors indicate an overlap of energy values of the PVP and no PVP HGNs analyzed.

synthesized without PVP possess narrower FWHMs and show absorption maxima at 600 nm, while ninety percent of synthesis with PVP resulted in HGNs that show a maximum absorption near 800 nm. It should be noted as well that when PVP was added to the HGN solution subsequent to synthesis, no shift in SPR was observed.

Representative low and high resolution TEM images obtained from HGN samples give valuable crystallographic detail. Fig. 3a shows HGNs synthesized without PVP, which reveals thick gold shells and large size heterogeneity. On the contrary, Fig. 3b shows HGNs synthesized with 500 μL of PVP, exhibiting ultra-thin gold shells, with an outer diameter of 32 ± 3.4 nm and a shell thickness of 3.2 ± 0.7 nm, a standard deviation of 10% and 21%, respectively. HRTEM images in Fig. 3c and d show a significant number of single crystalline domains with different orientations and lattice spacings indicating a polycrystalline structure. The [111] (2.3 Å) and [200] (2 Å) lattice fringes confirm the presence of crystalline fcc Au.[44]

To better understand the effect of PVP on the HGN synthesis, its concentration was systematically changed. Fig. 4a shows TEM images of a sample with 900 μL of PVP; HGNs are present individually, but also as more organized assemblies, including

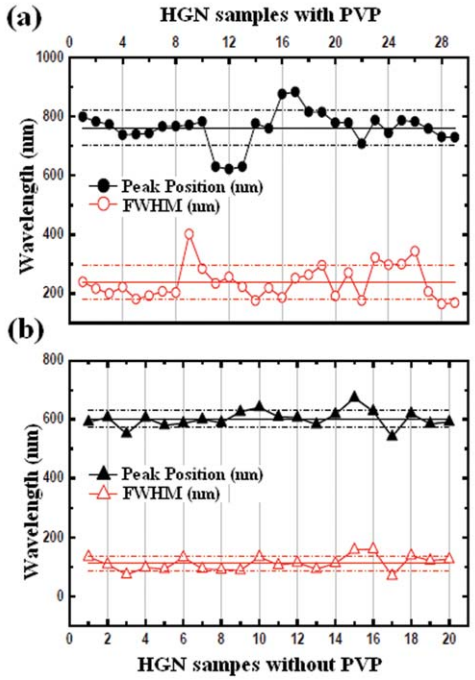

Fig. 2 Correlation between maximum absorption position and FWHM values with standard deviation for HGN samples with and without PVP.

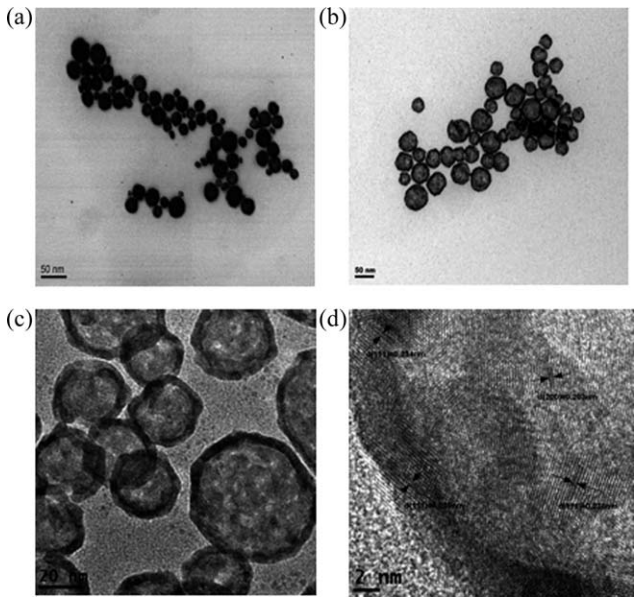

Fig. 3 TEM images of hollow gold nanospheres without PVP (a) and with 500 μL of PVP (b). The HGNs synthesized with PVP show isolated nanospheres with diameter of 32 ± 3.4 nm and 3.2 ± 0.7 nm in shell thickness. HRTEM images (c) and (d) of HGNs synthesized with PVP show the polycrystalline nature of gold shells with [111] and [200] Au lattice planes.

backbone-like structures with spaces of ~3 nm between HGNs, which may help explain the relatively broad SPR, in comparison with other values reported for HGNs.[13] A similar arrangement has been reported in HGNs with Co nanoparticles as templates, in which gold tubes with a continuous hollow interior[37,45] were

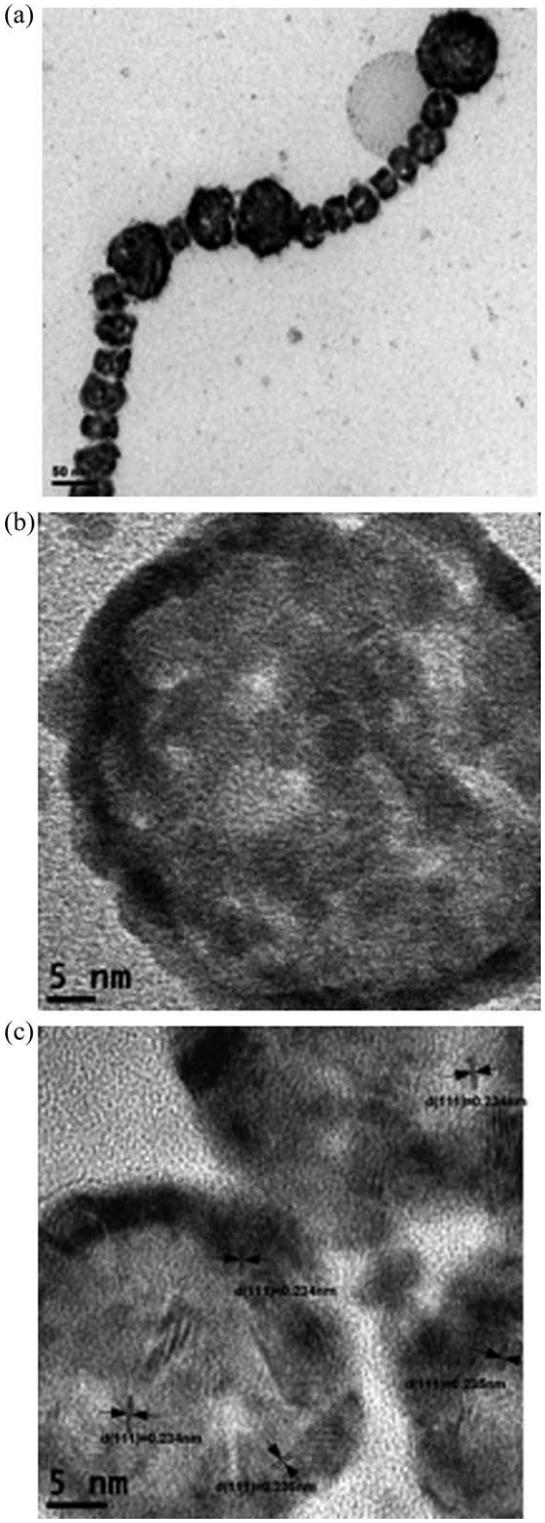

Fig. 4 TEM and HRTEM images of hollow gold nanospheres with 900 μL of PVP. (a) The alignment of HGNs with spaces of ~3 nm in a backbone-like structure; (b) a high resolution image of an isolated sphere with diameter of 31 ± 7.2 nm and 5.8 ± 1.3 nm in thickness, and (c) different HGNs with the [111] Au lattice planes.

formed due to the presence of an external magnetic field during the oxidation of cobalt that aligned the aggregating Co nanoparticles. Here, the ferromagnetic properties of cobalt, in

conjunction with the presence of PVP on the Co nanoparticles that interact with each other,[46] result in the ordered structures with regular separations that have not been seen before in the HGN synthesis without PVP.

The backbone-like structures are likely made up of HGNs truncated on two sides, that is, particles that look like rings when observed in broken backbone structures. This is explained by a dense solvating shell of coordinating PVP,[47] which both induces some weak interactions between the Co particles (causing the backbone formation) and protects the surface and slows the reaction of the Co metal with Au salt. While Au can clearly diffuse through the PVP, the reaction at the outer surface of the Co particles is kinetically more accessible than the interstitial space of the chain. Therefore, the gold shell forms preferentially along the transverse axis of the particle chain, forming gold rings, instead of connected nanotubes, as shown in previous works.[45]

The effect of PVP concentration on supra-particle organization can clearly be seen when comparing particles synthesized with 500 μL (Fig. 3b) and 900 μL (Fig. 4a) of PVP. At the lower concentration, only dispersed HGNS are observed. At this concentration it is likely that there is enough PVP to fully passivate the Co particles, but not enough to induce further agglomeration. At the higher concentration, TEM images are predominately populated with the organized backbone structures, indicating that PVP plays a strong role in inter-HGN interactions.

Fig. 4b shows a representative HRTEM image of HGNs synthesized at high PVP concentration. Fig. 4c is an additional HRTEM of the same sample with the [111] lattice planes for gold indicated. From these two HRTEM images, it is clear that at higher PVP concentrations the formation and resulting structure of the gold shell are strongly affected. In Fig. 3c the shells appear relatively uniform and even, whereas the present figure shows an uneven and porous structure. This being said, it is interesting that despite these structural differences in the shells and the predominant presence of backbone structures, the FWHM and SPR position are relatively unchanged. It is not clear at this time why this is the case, however, refinements to the synthesis are being made and we will attempt to answer some of these questions in future work.

Based on the fact that PAA and PEG do not allow HGNs with NIR SPR to be generated and only PVP does, it is clear that PVP possesses some unique molecular features that are important for the HGN synthesis. While the exact nature is not clear at this point and calls for further research, we would like to offer some possible explanations here. The individual acrylic acid units that comprise the polymer form of PAA have a pK_a of 4.25.[48] Therefore, near a neutral pH, there will be at least 500 times more of the negatively charged deprotonated form of the acid than the neutral protonated form. In weakly basic conditions, as is the case for our $CoCl_2$ and sodium citrate solution, there should be an even greater population of the negatively charged deprotonated form. Hence, it is likely that PAA will experience repulsion from negatively charged citrate-capped Co nanoparticles and would not be able to effectively interact with the Co nanoparticle surface. PEG, as a neutral species, would not experience Coulombic repulsion to prevent it from interacting with the Co surface; however, it is not predicted to have an especially strong affinity for the Co nanoparticle surface. In contrast, the amide moiety of PVP has shown to coordinate effectively with Co nanoparticles, serving as a stabilizing agent.[46] The stronger interaction is key to stabilizing the Co NPs and slowing down the Au nucleation and growth for producing large and thin gold shells.

In previous studies, PVP at high concentration (~mM) has been suggested as a reducing agent in the synthesis of silver and gold nanoparticles.[49,50] There is no evidence that the gold has been reduced at room temperature by PVP with the concentration used in our experimentation (μM), and this possibility is even less probable with the presence of much stronger reductants present in our HGN synthesis.

In addition, we have studied the effect of $NaBH_4$ concentration on the HGN synthesis by decreasing it from 1.0 M to 0.1 M in order to explore its possible influence along with the effect of PVP. It has been previously reported for HGNs that a lower $NaBH_4$ and citrate concentration results in larger cobalt particle size,[13] and larger Co particle diameters have greater possibility of templating HGNs with SPR in the NIR.[3,13] Since we have obtained HGNs with an SPR at NIR wavelengths in 12 syntheses, a lower concentration of $NaBH_4$ (0.1 M) and different amounts of PVP (100–900 μL) were performed in 17 more syntheses. Representative TEM images of some of these HGNs are shown in Fig. 5a and b. Fig. 5a is for HGNs obtained with

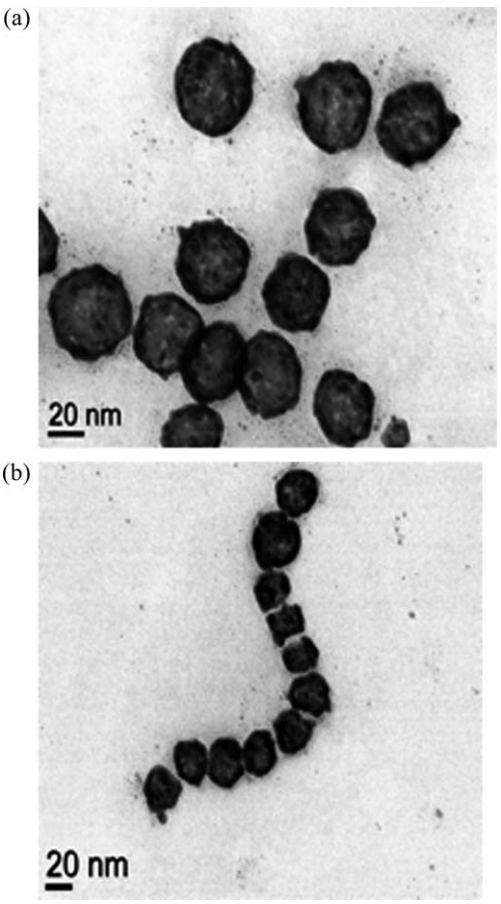

Fig. 5 TEM images of HGNs with 0.1 M of $NaBH_4$. (a) HGNs with 100 μL of PVP, 45 ± 4.0 nm in dia., thickness of 4.7 ± 0.8 nm and (b) HGNs with 700 μL of PVP, 36 ± 6.0 nm in dia., thickness of 4.0 ± 1.3 nm.

100 μL of PVP and the HGNs have an average outer diameter of 45 ± 4.0 nm and shell thickness of 4.7 ± 0.8 nm. Fig. 5b is for HGNs with 700 μL of PVP and the HGNs have an average outer diameter of 36 ± 6.0 nm and shell thickness of 4.0 ± 1.3 nm. While HGNs have been generated with similar reproducibility at low $NaBH_4$ concentration as at high concentration, the FWHM of the SPR is narrower (~250 nm) for 0.1 M than for 1.0 M $NaBH_4$ (~300 nm). This indicates that the HGNs at lower $NaBH_4$ concentration have better uniformity in size and shell thickness distribution.

It is important to remark that all samples have presented a size range suitable to extravasate and accumulate in tumors for cancer therapy treatments or for intracellular detection and imaging with SERS.[51,52] In addition, the optical properties of these HGNs make them particularly promising for biological applications where NIR light is of particular interest due to its extensive penetration depth and low interaction in tissue.

Conclusions

Highly reproducible and facile synthesis of 800 nm absorbing HGNs using PVP as template stabilizing agent has been demonstrated in the present work. PVP most likely slows down the nucleation and gold growth process, which makes it easier to produce thin shells that are necessary for generating SPR at desired NIR wavelengths, particularly 800 nm. Other polymers such as PAA and PEG do not promote the synthesis of HGNs with NIR absorption, possibly due to their inability to effectively coordinate with Co particles. This indicates that the HGN growth depends on the delicate interaction between the polymer and the Co nanoparticle template as well as gold. Further research is needed to better understand the details of the interaction. Future work is also needed to address the control of the uniformity of the shell and the shape of the HGNs, which will help to narrow the SPR bandwidth. This will be important in improving the performance of HGNs in applications such as SERS for chemical and biochemical detections as well as photothermal ablation therapy as an effective technique for cancer treatment.

Acknowledgements

This work is supported by the National Science Foundation. S. Preciado-Flores acknowledges a postdoctoral fellowship grant from CONACyT (Mexico). Danchen Wang is grateful to the Chinese Scholars Council for support. Damon Wheeler was funded by W. M. Keck Center for Nano- and Optofluidics though a QB3 Fellowship. We are grateful for the use of the HRTEM facilities at the National Center Electron Microscopy, Lawrence Berkeley National Lab., which is supported by the US Department of Energy under contract number DE-AC02-05CH11231and Chenyou Song for his assistance. We thank Carley Corrado for stimulating discussions and Gongming Wang for help on the HRTEM analysis.

References

1 C. F. Bohren, *Am. J. Phys.*, 1983, **51**, 323–327.
2 J. A. Creighton and D. G. Eadon, *J. Chem. Soc., Faraday Trans.*, 1991, **87**, 3881–3891.
3 E. Hao, S. Y. Li, R. C. Bailey, S. L. Zou, G. C. Schatz and J. T. Hupp, *J. Phys. Chem. B*, 2004, **108**, 1224–1229.
4 J. Z. Zhang and C. Noguez, *Plasmonics*, 2008, **3**, 127–150.
5 S.-S. Char, C.-W. Shih, C.-D. Chen, W.-C. Lai and C. Wang, *Langmuir*, 1999, **15**, 701–709.
6 N. R. Jana, L. Gearheart and C. J. Murphy, *J. Phys. Chem. B*, 2001, **105**, 4065–4067.
7 S. H. Im, Y. T. Lee, B. Wiley and Y. Xia, *Angew. Chem.*, 2005, **117**, 2192–2195.
8 A. J. Haes, W. P. Hall, L. Chang, W. L. Klein and R. P. Van Duyne, *Nano Lett.*, 2004, **4**, 1029–1034.
9 S. E. Skrabalak, L. Au, X. M. Lu, X. D. Li and Y. N. Xia, *Nanomedicine*, 2007, **2**, 657–668.
10 T. J. Norman, C. D. Grant, D. Magana, J. Z. Zhang, J. Liu, D. L. Cao, F. Bridges and A. Van Buuren, *J. Phys. Chem. B*, 2002, **106**, 7005–7012.
11 M. A. Mahmoud and M. A. El-Sayed, *Nano Lett.*, 2009, **9**, 3025–3031.
12 Y. Xia, B. Gates, Y. Yin and Y. Lu, *Adv. Mater.*, 2000, **12**, 693–713.
13 A. M. Schwartzberg, T. Y. Olson, C. E. Talley and J. Z. Zhang, *J. Phys. Chem. B*, 2006, **110**, 19935–19944.
14 S. J. Oldenburg, R. D. Averitt, S. L. Westcott and N. J. Halas, *Chem. Phys. Lett.*, 1998, **288**, 243–247.
15 S. J. Oldenburg, G. D. Hale, J. B. Jackson and N. J. Halas, *Appl. Phys. Lett.*, 1999, **75**, 1063–1065.
16 Y. G. Sun, B. T. Mayers and Y. N. Xia, *Nano Lett.*, 2002, **2**, 481–485.
17 Y. G. Sun and Y. N. Xia, *Anal. Chem.*, 2002, **74**, 5297–5305.
18 H. P. Liang, L. J. Wan, C. L. Bai and L. Jiang, *J. Phys. Chem. B*, 2005, **109**, 7795–7800.
19 T. Y. Olson, A. M. Schwartzberg, C. A. Orme, C. E. Talley, B. O'Connell and J. Z. Zhang, *J. Phys. Chem. C*, 2008, **112**, 6319–6329.
20 A. M. Schwartzberg, T. Y. Oshiro, J. Z. Zhang, T. Huser and C. E. Talley, *Anal. Chem.*, 2006, **78**, 4732–4736.
21 S. Liu, J. Liu, X. Han, Y. Cui and W. Wang, *Biosens. Bioelectron.*, 2010, **25**, 1640–1645.
22 M. P. Melancon, W. Lu, Z. Yang, R. Zhang, Z. Cheng, A. M. Elliot, J. Stafford, T. Olson, J. Z. Zhang and C. Li, *Mol. Cancer Ther.*, 2008, **7**, 1730–1739.
23 W. Lu, C. Xiong, G. Zhang, Q. Huang, R. Zhang, J. Z. Zhang and C. Li, *Clin. Cancer Res.*, 2009, **15**, 876.
24 J. Z. Zhang, *J. Phys. Chem. Lett.*, 2010, **1**, 686–695.
25 R. Bardhan, N. K. Grady, J. R. Cole, A. Joshi and N. J. Hallas, *ACS Nano*, 2009, **3**, 744–752.
26 Y. Lu, Y. Zhao, L. Yu, L. Dong, C. Shi, M.-J. Hu, Y.-J. Xu, L.-P. Wen and S.-H. Yu, *Adv. Mater.*, 2010, **22**, 1407–1411.
27 M. Gellner, B. Küstner and S. Schlücker, *Vib. Spectrosc.*, 2009, **50**, 43–47.
28 D. A. Ferrer, L. A. Diaz-Torres, W. Shaomin and M. Jose-Yacaman, *Catal. Today*, 2009, **147**, 211–216.
29 R. Bardhan, W. Chen, C. Perez-Torres, M. Bartels, R. M. Huschka, L. L. Zhao, E. Morosan, R. G. Pautler, A. Joshi and N. J. Halas, *Adv. Funct. Mater.*, 2009, **19**, 3901–3909.
30 B. D. Chithrani, A. A. Ghazani and W. C. W. Chan, *Nano Lett.*, 2006, **6**, 662–668.
31 S. J. Oldenburg, J. B. Jackson, S. L. Westcott and N. J. Halas, *Appl. Phys. Lett.*, 1999, **75**, 2897–2899.
32 C. Graf, D. L. J. Vossen, A. Imhof and A. Van Blaaderen, *Langmuir*, 2003, **19**, 6693–6700.
33 A. Guerrero-Martínez, J. Pérez-Juste and M. Liz-Marzán, *Adv. Mater.*, 2010, **22**, 1182–1195.
34 E. Díaz, R. B. Valenciano and I. A. Katime, *J. Appl. Polym. Sci.*, 2004, **93**, 1512–1518.
35 R. Harder, M. Liang, Y. Sun, Y. Xia and I. K. Robinson, *New J. Phys.*, 2010, **12**, 035019.
36 Y. Sun and Y. Xia, *Science*, 2002, **298**, 2176–2179.
37 J. Zeng, J. Huang, W. Lu, X. Wang, B. Wang, S. Zhang and J. Hou, *Adv. Mater.*, 2007, **19**, 2172–2176.
38 C. Li, K. L. Shuford, Q.-H. Park, W. Cai, Y. Li, E. J. Lee and S. O. Cho, *Angew. Chem.*, 2007, **119**, 3328–3332.
39 C. S. Ah, Y. J. Yun, H. J. Park, W.-J. Kim, H. D. Han and X. Yun-Jun, *Chem. Mater.*, 2005, **17**.
40 W. S. Rasband, *ImageJ*, 1997–2009, http://rsb.info.nih.gov/ij/.
41 A. M. Schwartzberg, T. Y. Olson, C. E. Talley and J. Z. Zhang, *J. Phys. Chem. B*, 2006, **110**, 19935–19944.
42 J. Z. Zhang and C. Noguez, *Plasmonics*, 2008, **3**, 127–150.

43 E. Prodan, C. Radloff, n. J. Halas and P. Nordlander, *Science*, 2003, **302**, 419.
44 M. Brust, J. Fink, D. Bethell, D. J. Schiffrin and C. Kiely, *J. Chem. Soc., Chem. Commun.*, 1995, 1655–1656.
45 A. M. Schwartzberg, T. Y. Olson, C. E. Talley and J. Z. Zhang, *J. Phys. Chem. C*, 2007, **111**, 16080–16082.
46 Y. Xiong, Q. Chen, N. Tao, J. Ye, Y. Tang, J. Feng and X. Gu, *Nanotechnology*, 2007, **18**, 345301–345305.
47 W. Shao, Y. Huang, H. Lee, Y. J. Suh and C. O. Kim, *Curr. Appl. Phys.*, 2006, **6**, e195–e197.
48 D. R. Lide, *CRC Handbook of Chemistry and Physics*, Editorial Advisory Board, 2006–2007.
49 C. Li, J. Mei, S. Li, N. Lu, L. Wang, B. Chen and W. Dong, *Nanotechnology*, 2010, **21**, 245602–245608.
50 C. Hoppe, M. Lazzari, I. Pardinas-Blanco and M. A. Lopez-Quintela, *Langmuir*, 2006, **22**, 7027–7034.
51 A. M. Schwartzberg and J. Z. Zhang, *J. Phys. Chem. C*, 2008, **112**, 10323–10337.
52 D. P. O'Neal, L. R. Hirsch, N. J. Halas, J. D. Payne and J. L. West, *Cancer Lett.*, 2004, **209**, 171–176.

